Technical Article

Degradation Mechanisms of APS and EB-PVD Thermal Barrier Coatings

A. Rabieifar*[,1], V. Abouei Mehrizi[1], M. Ghanbari Haghighi[1]

[1]Advanced Materials Engineering Research Center, Karaj Branch, Islamic Azad University, Karaj, Iran.
Received: 14 February 2023 - Accepted: 30 May 2023

Abstract

Thermal barrier coatings (TBCs) are a crucial technology in thermal stability. Their use to achieve surface temperature reduction of the underlying superalloys surpasses all other achievements in the field of material technologies that have taken place in the last three decades. The technological advances in TBCs make them suitable for operation in the most demanding high-temperature environment of aircraft and industrial gas-turbine engines. The performance of these multi-layered and multi-material systems, tailored for high-temperature applications, is closely linked to their microstructure evolution. Many factors influence the durability of TBCs; therefore, in order to tailor these engineering materials for high-temperature applications, it is required to have a comprehensive understanding of the effects of the contributing factors and their interaction with the development of advanced TBCs. Improvements in TBCs will require a better understanding of the complex changes in their structure and properties that occur under operating conditions that lead to their failure. This article overviews the intrinsic and extrinsic degradation mechanisms, including TGO growth, thermal shock, CMAS attack, hot corrosion, erosion, sintering and phase transformations, thermal fatigue, thermo-mechanical tensile and foreign object damage.

Keywords: Thermal Barrier Coating, Air Plasma Spray, Electron-Beam Physical Vapor Deposition, Degradation Mechanism.

1. Introduction

Thermal barrier coatings (TBCs) are functional ceramic coatings with a low thermal conductivity applied onto nickel-based superalloys. With the successful application of these coatings, the operating temperature of high-temperature parts (stator/rotor) of land-based gas turbines and aircraft engines increases, increasing durability, performance, and efficiency [1]. A typical TBC system is composed of a layer of top coat (TC), which is commonly yttria-stabilized zirconia (YSZ), an oxidation-resistant bond coat (BC), and a creep-resistant, high-strength Ni-based superalloy transitional layer [2]. In the high-temperature environment, a thin oxide scale, i.e., thermally grown oxide (TGO, usually Al2O3), forms and grows between the TC and BC interface due to the oxidation of the BC layer [3]. A typical thermal barrier coating system used in combustor and turbine sections is shown in Fig. 1. By applying TBCs, the temperature and the driving force for the alloy substrates' thermal fatigue and creep failure are thus reduced, resulting in the durability of the substrates. The role of the ceramic top coat is to provide a thermal barrier and corrosion resistance. At the same time, the BC layer provides the adhesion between the metal substrate and ceramic TC and protection of the substrate from high-temperature corrosion and oxidation.

*Corresponding author
Email address: a.rabieifar@kiau.ac.ir

The coefficient of thermal expansion (CTE) of zirconia ($11–13\times10^{-6}$ ˚C) is low compared to that of metal substrates ($18–20\times10^{-6}$ ˚C), although it is higher than most ceramic materials. Thus, a NiPtAl diffusion or an MCrAlY overlay BC reduces the CTE mismatch between TC and the substrate. Based on the type of superalloy and different working environments, M can be any one of Co, Ni, CoNi, NiCo, or Fe [4]. TBCs experience the most-severe working environments in gas turbine engine operations regarding temperature and its gradient, non-uniformity in pressure and heating, oxidizing conditions, hot corrosion, mechanical loadings, and particle impact**.** Early damages develop in TBCs and grow with service time, leading to eventual failure. Many factors influence the durability of TBCs, such as imposed profiles of thermal load, a thermal mismatch at the interface of BC and TC, BC oxidation, sintering effects, inter-diffusion, phase transformation, surface undulation, and hot corrosion [5-8], and adhesion strength [9]. Therefore, during service conditions, each factor affects the induced internal stresses in the individual constituents differently, resulting in different failure modes in the system [10]. Hence, there is a need for a comprehensive understanding of the effects of the contributing factors and their interaction to develop advanced TBCs. As a thermal barrier, the TBC materials must also meet performance requirements, such as a high melting point, good corrosion resistance, no phase transformation during thermal cycling, good damage tolerance, a low sintering rate, and thermal

expansion matching with the metallic substrate. This paper reviewed degradation mechanisms that the TBC system might be subjected to during service life.

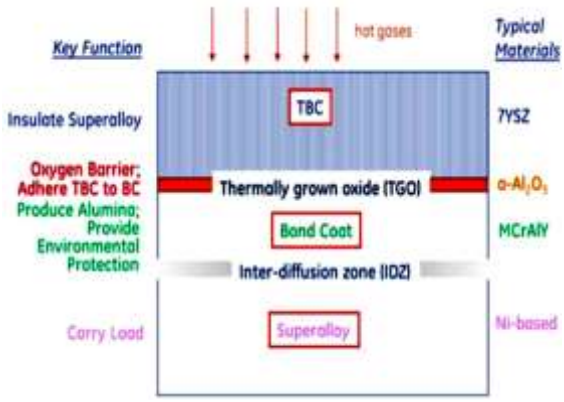

Fig. 1. Typical thermal barrier coating system used in combustor and turbine sections [11].

2. Deposition of TBC coatings

Two different methods are used for the production of the ceramic top coat: (i) electron-beam physical vapor deposition (EB-PVD) and (ii) air plasma spray (APS) [12–19]. As seen in Fig. 2. And Fig. 3., the main difference between these two methods is in the morphology of their microstructure. APS coatings have a lamellar microstructure, while EB-PVD coatings have a columnar microstructure. Thus, the ceramic top coat produced by the APS technique has lower thermal conductivity due to micro-porosities between the lamellae. On the other hand, micro-porosities between the columns provide higher expansion tolerances in the ceramic top coat produced by the EB-PVD technique. The APS process is more suitable for coating large parts and is cheaper than the EB-PVD process [20]. Static and stationary parts of the gas turbines are coated with a ceramic insulating material using the APS process.

2.1. Air Plasma Sprayed TBCs.

APS TBCs have the following favorable microstructural characteristics: (i) "splat" grain morphology (1 to 5 μm thick, 200 to 400 μm diameter) with inter-splat boundaries and cracks parallel to the metal/ceramic interface for low thermal conductivity and (ii) 15 to 25 vol.% porosity for both low elastic modulus (high strain tolerance) and low thermal conductivity. However, the undulating nature of the metal/ceramic interface, which is required for better interlocking adhesion, produces out-of-plane stresses responsible for the in-service failure of APS TBCs. A typical APS top coat is 300 μm thick, but in some industrial gas turbine engines, it can reach 600 μm in thickness. The orientation of the cracks and pores normal to the heat flow reduces the thermal conductivity of the TC [21]. However, because of the proliferation of microstructural defects parallel to the interface and the roughness of the interface, APS TBCs generally have shorter thermal cycling lives than EB-PVD TBCs. It makes APS TBC suitable only for less exacting applications in aircraft engines, such as combustors, fuel vaporizers, after-burner flame holders, and stator vanes. APS TBCs have served exceptionally well in industrial gas turbine engines, including blades and vanes applications, because of lower operating temperatures, reduced temperature gradients, and fewer thermal cycles [22].

2.2. Electron-beam physical vapor deposited TBCs.

In contrast to the APS case, the BC surface can be smooth before deposition. Typically, EB-PVD top coats (125 μm thick) have the following microstructural features: (i) thin region of polycrystalline YSZ with equiaxed grains (size 0.5 to 1 μm) at and near the metal/ceramic interface; (ii) columnar YSZ grains (2 to 10 μm diameter) growing out of the equiaxed-grain region to the top-coat surface; (iii) nanometer-scale porosity within the columnar grains; and (iv) channels separating the columnar grains, normal to the metal/ceramic interface. The disconnected columns impart strain tolerance to the TBC because they can separate at high temperatures, accommodating thermal expansion mismatch stresses [23]. The porosity and the cracks help reduce the thermal conductivity [24], but to a lesser extent than APS TBCs because the channels are parallel to the direction of heat flow. EB-PVD TBCs are more durable but expensive, relative to APS TBCs, and are used primarily in the most severe applications, such as turbine blades and vanes in aircraft engines.

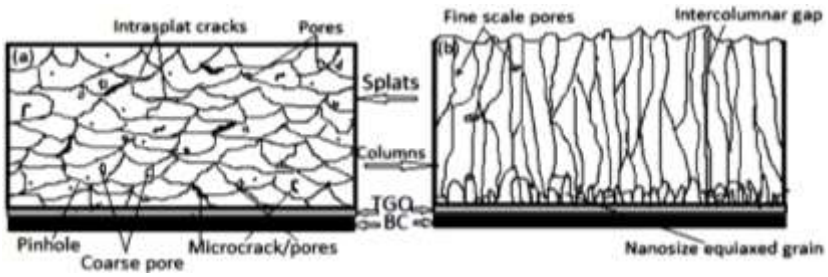

Fig. 2. Schematic illustration of as-deposited YSZ microstructures of (a) APS-TBC, (b) EB-PVD TBC. The essential features and various defects are displayed and labeled [25].

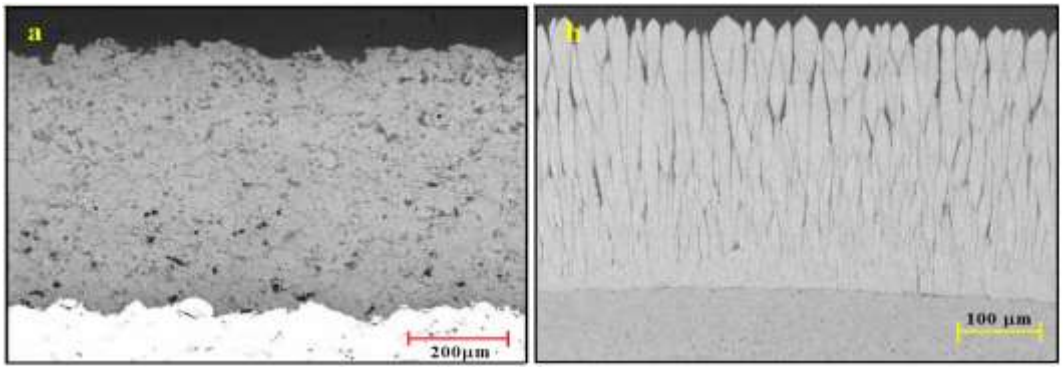

Fig. 3. (a) APS-TBC with a layered network of inter-connected splats, (b) EB-PVD TBC with a columnar microstructure [26].

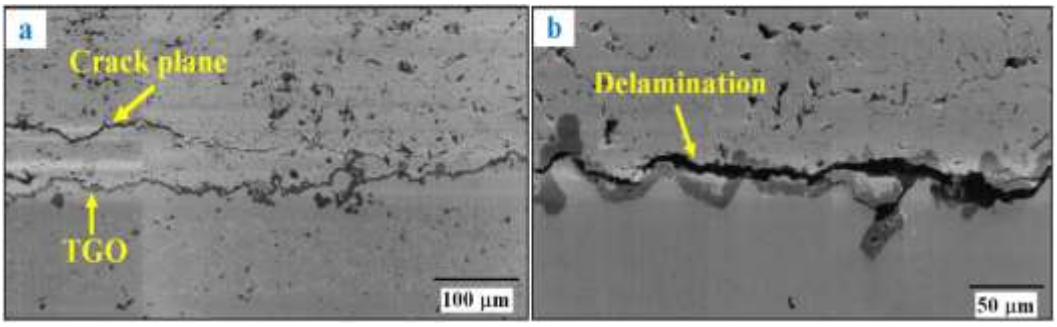

Fig. 4. SEM images of delaminations induced by wedge impressions, (a) sample with 3 μm thick TGO; (b) sample with 7 μm thick TGO [28].

3. Intrinsic Failure Mechanisms of YSZ TBC

3.1 Degradation From TGO Growth

Many factors contribute to the applied stresses within APS-TBC, such as YSZ structure, the microstructure of TGO, TGO growth at an undulating BC/TC interface, chemical compositions of BC, surface roughness, thermal expansion mismatch, and the formation of spinel/mixed oxides due to Al-depletion in the BC. However, the strain and stress induced by the growth of TGO are the prominent factors failing TBCs [27, 28]. The SEM images of delaminations induced by wedge impressions in different TGO thicknesses are shown in Fig. 4. Beyond 700 ˚C, the BC is oxidized, and the TGO layer is formed between BC and YSZ [29]. It is preferred to have an α-Al_2O_3-based TGO layer rather than other mixed oxides because the outward diffusion of metal elements can be effectively reduced [30]. The growth of the TGO can be divided into three stages: a transient stage, when all thermodynamically stable oxides can form (e.g., α-Al_2O_3, Cr_2O_3, CoO, NiO); a steady-state stage, when the high temperature stable, long-term phase (α-Al_2O_3) is established and grows; and finally a breakaway stage, when the growth of less protective oxides (spinel oxides) leading to the failure of the scale [31, 32]. The α-Al_2O_3 phase is the ideal TGO component among these oxides due to exhibiting the lowest ion diffusion rate and best thermal stability. Compared with other TGO compositions, TGO composed of α-Al_2O_3 shows more excellent oxidation resistance of BC [30]. As a result of the significant value of thermal expansion differences between the TGO layer and the substrate, the formation of oxides and their growth lead to spallation and the failure of the TBC [29]. The oxidation kinetics of TGOs usually follows a parabolic equation. It is noticed that the stress intensity, stress distribution, and interface structure can be significantly altered by the TGO growth [33]. The depletion of Al in BC is the consequence of the growth of the α-Al_2O_3-based TGO. The severe Al depletion would lead to the formation of other oxides like Y_2O_3, $Y_3Al_5O_{12}$, and CSN (Cr_2O_3, NiO, spinel) oxides. As a result, the structural integrity of TGO is impaired, fast oxygen diffusion paths are provided, and localized oxidation is accelerated [34]. By falling the Al concentration below a critical value, α-Al_2O_3 is no longer the preferred thermodynamic phase, and other oxides, notably spinels, form [35]. Bulky oxide clusters containing CSN oxides are shown in Fig. 5. As can be seen in Fig. 6, due to the high growth rate of CSN oxides compared to Al_2O_3, the thickness of the TGO layer at the place of formation of these oxides has increased locally and has led to the convexity of the TGO layer. These other oxides do not form such a protective scale; consequently, the alloy oxidizes faster. In addition,

the formation of these oxides is associated with an increase in volume that can be disruptive and possibly have lower fracture energies. Nevertheless, there are reports that failure follows such aluminum depletion when the BC is porous and at low-oxidation temperatures [36].

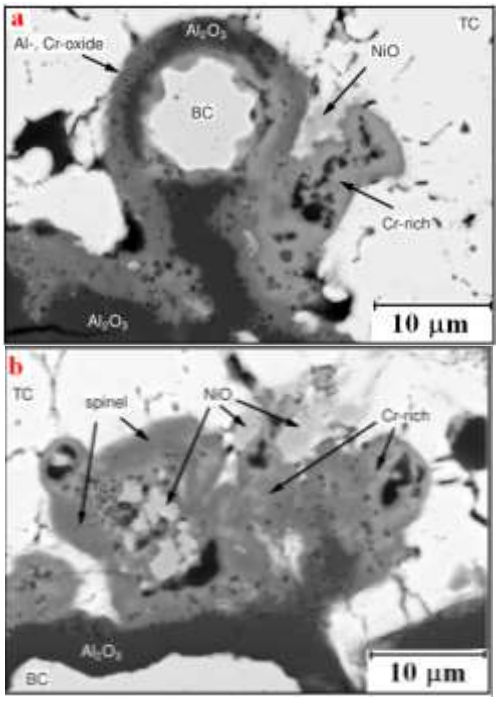

Fig. 5. Backscatter electron images showing bulky oxide clusters, TCF 300 cycles, (a) Small metallic BC particles sticking out in the TC, rapidly oxidizing and forming an oxide cluster. (b) An oxide cluster with a core of NiO [38].

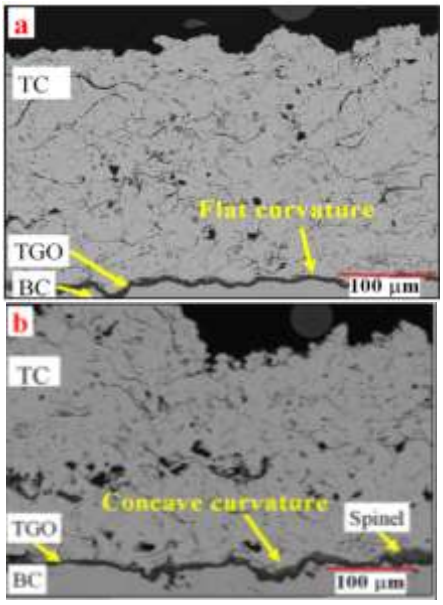

Fig. 6. SEM images of TC, TGO and spinels in specimens exposed at 925 ˚C for 7000 h. (a) location with flat curvature and (b) location with concave curvature [27].

Although related to the oxidation behavior of the BC, neither the concept of a critical thickness nor aluminum depletion can account for the wide distribution in failure lives, especially under thermal cycling conditions. Indeed, in most materials examined after failures above about 1000 ˚C, the aluminum concentration, although depleted somewhat, has not fallen to the critical value [37].

3.1.1. Buckling Instability

One of the failure modes is that the part of the coating buckles and spalls away from the alloy, typically cooling down to room temperature [39]. A typical buckling failure is illustrated in Fig. 7. Such buckling and subsequent spallation is a common mode of failure of all films and coatings under compression, generally associated with the development of compressive residual stresses in the coatings as a result of the difference in CTE between the coating and the underlying alloy. The failure's mechanics by buckling a thin, elastically isotropic film under compression from a flat surface is well understood [40], provided an un-bonded region of a critical size, d_b, and exists at the interface (Fig. 8). For example, in NiPtAl/YSZ coating, the surface of the BC roughens in Fig. 9. for coating after cyclic thermal exposure, and separations form with the TBC even though the bottom surface of the TBC remains flat. These separations are interface flaws that progressively grow in size and link with adjacent ones to allow buckling and spallation [41]. Roughening is more pronounced with thermal cycling but occurs more slowly on isothermal exposures [42]. At least two new mechanisms have been identified that can lead to such roughening. The roughening has been attributed to a “ratcheting” phenomenon motivated by the lateral compressive stress in the growing TGO and facilitated by thermal cycling [22]. Measurements indicate that as the TGO grows thick with oxidation, it also concurrently develops compressive stress [43, 44]. If it were free to expand, it would decrease its compressive stress, but because it is attached to the BC, the only way in which it can reduce its elastic strain energy is by undulating (Fig. 10). In this way, its length increases and it remains attached to the alloy. This undulation requires the alloy to deform to accommodate the undulation, and the oxide must also deform concurrently. According to the ratcheting mechanism, this accommodation is by plastic deformation of both the TGO and BC during thermal cycling. As the lateral growth of the thickening oxide continues during the high-temperature portion of the thermal cycles, it continues to generate compressive stress that is relaxed by ratcheting during the thermal cycle, so the process is ongoing.

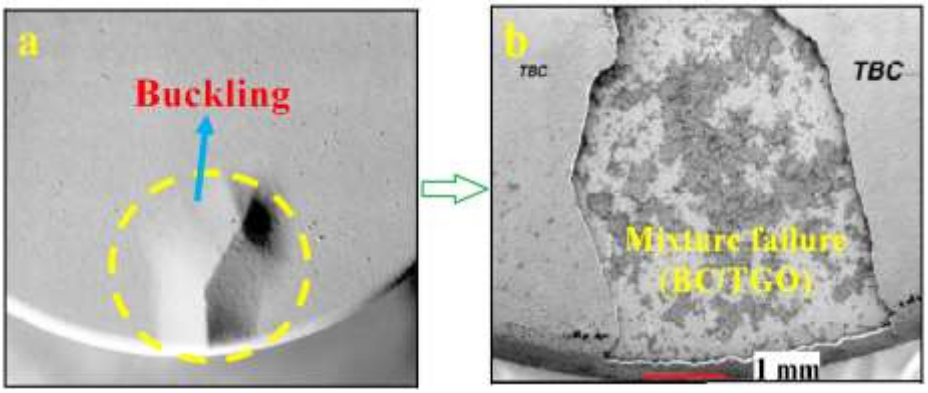

Fig. 7. (a) Incipient buckling of a TBC coating viewed under reflected light. (b) The failure surface revealed by spallation of the TBC consists of a mixture of local failure between the TGO and the BC (appearing dark) and in the TBC itself (light regions) [45].

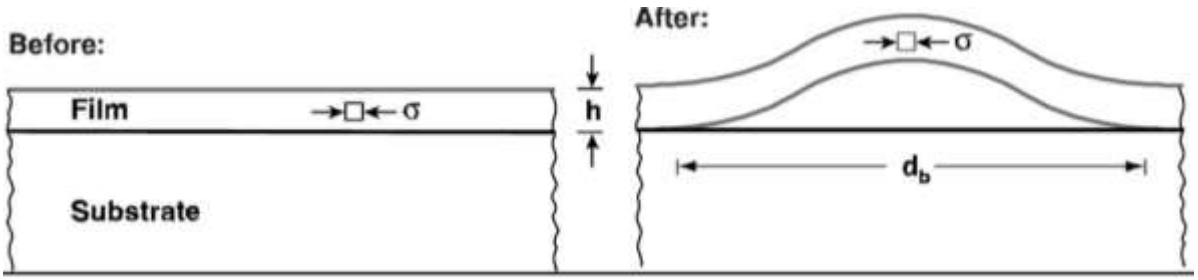

Fig. 8. Schematic illustration of the buckling of a compressed film above a pre-existing defect of diameter d_b [45].

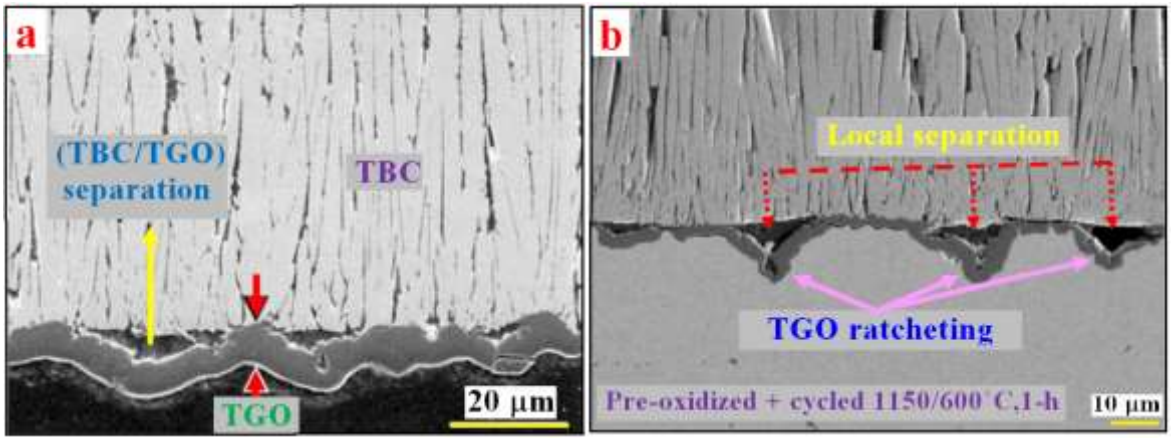

Fig. 9. (a) Local separation between the TBC and the BC after thermal cycling. (b) The BC/TC interface separations indicate the underlying BC has changed its surface morphology during high-temperature thermal cycling [45].

Another new mechanism shown to cause roughening is the surface displacement associated with volumetric changes in the BC as aluminum depletion occurs. This roughening is illustrated in Fig. 11, together with etched cross-sections revealing the presence of both γ′ and β phases in the BC [42]. After aluminizing and YSZ deposition, the PtNiAl-BC is chemically homogeneous and has the β-NiAl (B2) crystal structure.

After high-temperature exposure, the initially flat BC is rumpled, and etching reveals that the BC has partially transformed to γ′-Ni_3Al. In addition, the remaining β-NiAl phase regions often have the characteristic lath structure of Martensite. These two observations can be understood as the result of aluminum depletion from the BC and the concurrent enrichment of nickel from the underlying superalloy, a classic example of inter-diffusion.

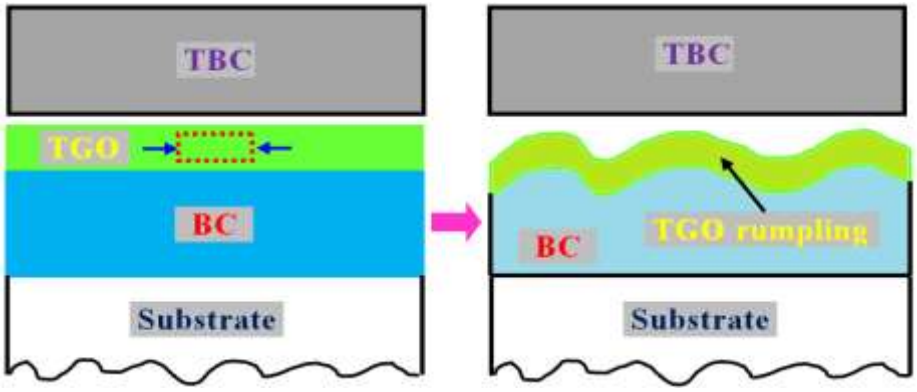

Fig. 10. Schematic illustration of how an initially flat but compressed film (a) can lower its elastic strain energy by rumpling (b). The amplitude of rumpling is enhanced by thermal cycling and can cause interface separation if a superimposed coating cannot deform to follow the displacements of the film [46].

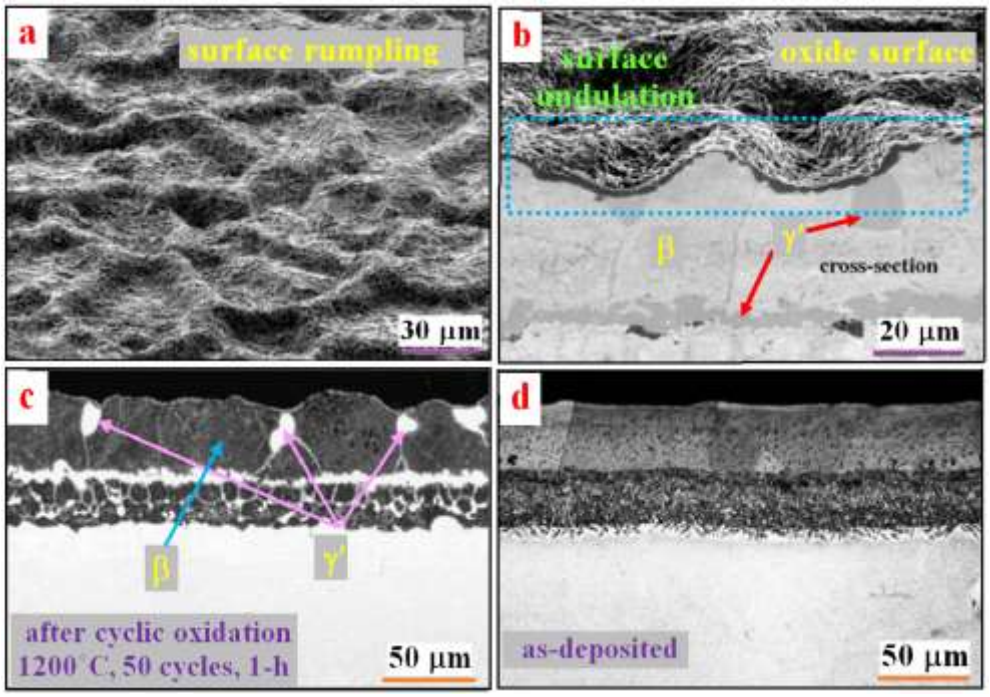

Fig. 11. Microstructure of an initially flat as-aluminized BC after 50 1-h cycles at 1200 °C, (a) surface rumpling; (b) cross-section showing an instead uniform oxide layer and strong surface undulations (γ′-phase is revealed by etching); (c, d) optical micrographs showing etched cross-sections before and after cyclic oxidation. Dark areas on the optical images correspond to the β-phase, whereas the γ′ phase in the coating appears white [42].

3.1.2. Cracking Failure in APS-TBC

At least four primary failure mechanisms in APS TBCs are driven by the out-of-plane stresses, shown schematically in Fig. 12.a [47, 48]. The BC/TGO interface stresses are tensile at the undulation crests and compressive at the troughs [49]. As the TGO thickens, the tensile stress increases, which causes cracking at the BC/TGO interface at crests (mechanism I in Fig. 12.a, Fig. 12.b) [50]. The CTE mismatch between the TC and the metal (BC/superalloy) puts the TC in overall compression at room temperature. However, these stresses are an order of magnitude lower than the residual stresses in the TGO, primarily because the porous and cracked TC is much more compliant than the TGO and has a relatively lower CTE mismatch with the BC. Once again, because of the highly undulating nature of the metal/ceramic interface, out-of-plane stresses result in the vicinity of the TGO/TC interface: tension at the crests and compression at the troughs [51]. The tension causes fracture along the TGO/TC interface at the crests (mechanism II in Fig. 12.a, Fig. 12.b) and cracking within the highly brittle TC in the vicinity of the crests (mechanism III in Fig. 12.a, Fig. 12.b) [48]. As the TGO thickens, it constitutes a good fraction of the BC asperity. Thus, the thermal stresses are locally dominated by the CTE mismatch between the BC/TGO composite asperity rather than just the BC and the TC. Beyond a certain TGO thickness,

the CTE of the BC/TGO composite becomes lower than that of both the TC and the BC, which reverses the nature of the stresses in the TC undulation troughs from compression to tension [48, 52]. This reversal causes cracking within the TC in the valleys between the crests (mechanism IV in Fig. 12.a, Fig. 12.b) [48].

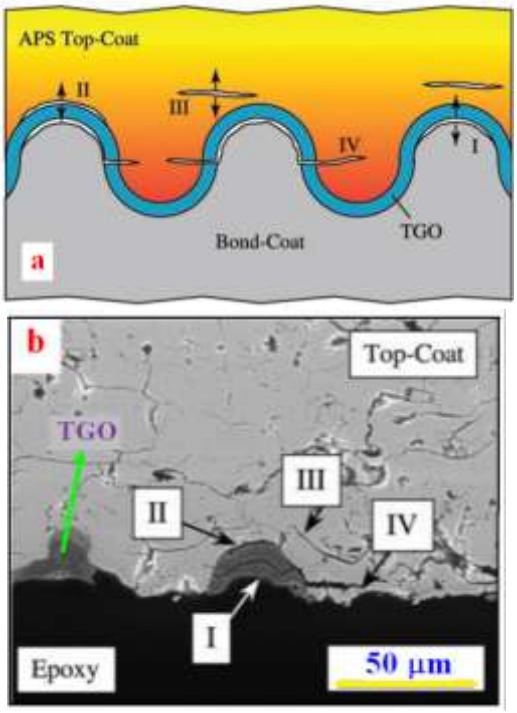

Fig. 12. (a) Schematic diagram showing the four different cracking mechanisms in APS TBC, (b) Cross-sectional SEM of a failed APS TBC (240 cycles) mounted in epoxy (bond-coated substrate not shown) showing the various cracking mechanisms illustrated in (a) [22].

3.1.3. Cracking failure in EBPVD-TBC

Because the TC in EB-PVD TBCs is more strain tolerant than that in APS TBCs, the various cracking events in this system occur at the BC/TGO or the TGO/TC interfaces. There are three main types of failure mechanisms in this system, two of which are schematically shown in Fig. 13.a. Mechanism I, separation of the BC/TGO interface, is the same as that described in the APS TBC case (mechanism I in Fig. 12). The crests in the case of EB-PVD are ridges present on the BC surface before TC deposition (Fig. 13.b) [53]. Mechanism II in Fig. 13.a is the separation of the TGO/TC interface and penetration of the TGO into the BC resulting from one or more of the following mechanisms: (i) progressive TGO roughening caused by BC cyclic creep (Fig. 13.b, Fig. 13.c) [54, 55]; (ii) accelerated growth of embedded oxides due to localized TGO cracking [56-58]; and (iii) cavity formation in the BC [55]. For EB-PVD TBCs with relatively flat and defect-free interfaces, the compression in the TGO causes large-scale buckling, as shown in Fig. 13.d [53, 59].

3.2. Cyclic Creep

The rotation of turbine blades is in the air at high speed at high temperatures; therefore, TBCs are subjected to mechanical loads and thermal cycles. According to investigations, the main factor for interfacial cracking is the unstable TGO layer subjected to thermal cycling. As stated in the previous section, the growth of TGO, in addition to creating waviness on its surface, leads to the production of compressive and tensile residual stresses in different areas of the BC/TGO interface [60]. The TGO instability generates strains in TBCs. Moreover, the strains resulting from the TGO growth and CTE mismatch are superimposed. However, stress relaxation occurs due to the micro-cracks and plastic deformation within the TC. The stress level is reduced due to plastic deformation and material creep at high temperatures. Meanwhile, TGO instability is promoted by micro-cracks and plastic deformation. It can accumulate stress upon thermal cycling, which motivates early cracking at TGO/BC and TGO/TC interfaces [61]. As a result of the cyclic creep of the BC during thermal cycling, the roughening of the BC/TGO/TC interfaces (ratcheting) occurs progressively and is seen in thermal cycling conditions rather than isothermal exposures. It is also required to have some initial surface imperfection of minimum size and a progressive increase in the TGO length because of in-plane growth during oxidation or TGO cracking. This roughening in flat BC/TGO interface of EB-PVD TBC is in the form of penetration of TGO into BC. The roughening appears in the amplified undulation amplitude in APS TBC, in which the interface is undulated [34]. Under slow creep rate conditions, the damage develops at one of the TGO interfaces (Fig. 14.b). Hence, upon progressive oxidation of the BC, a progressive transfer of the critical locations (i.e., locations where cracks will preferentially develop) from the substrate/BC interface to the BC/TGO or TGO/TC interface is observed. One of the reasons for such a delamination process at the BC/substrate interface (Fig. 14.a) is the reduction in the load-bearing section due to the creep deformation of the substrate. In the preferential locations, the radial and tangential stresses are due to a locking effect of the columns of the TC, stresses which cannot be infinitely relaxed by the visco-plastic flow of the BC. In addition, under such conditions of high creep rate, microstructural defects at the substrate/BC interface are critical in controlling the nucleation of cracks because they act as stress concentrators [62].

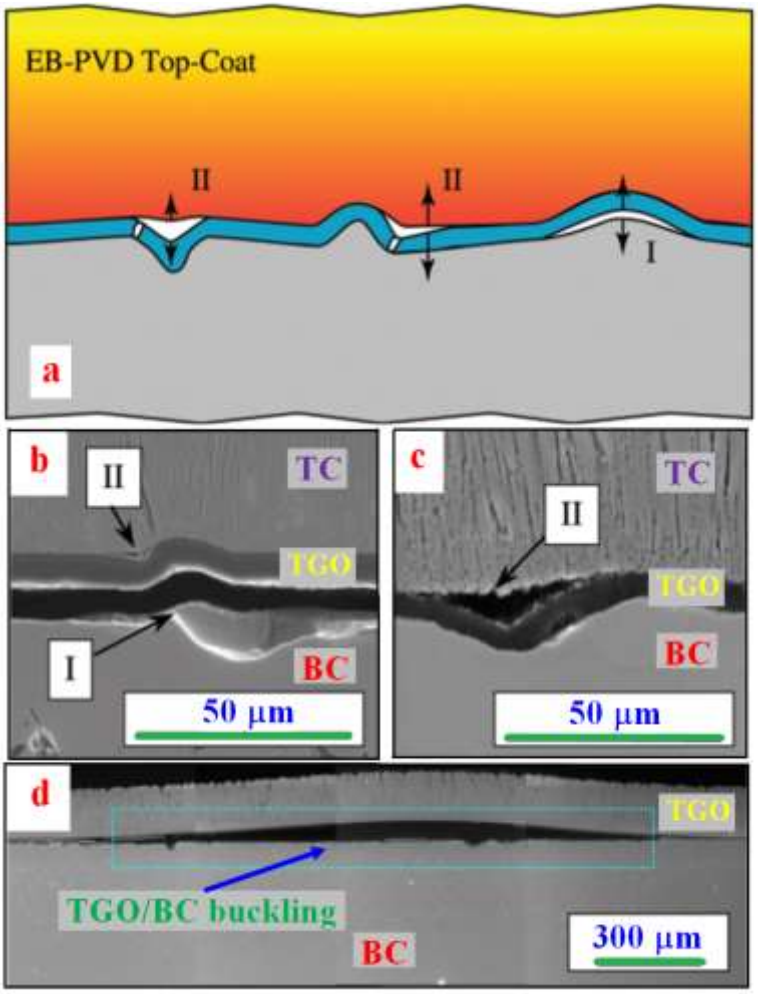

Fig. 13. (a) Schematic diagram showing two of the three different cracking mechanisms in EB-PVD TBC. Cross-sectional SEMs showing, (b) mechanisms I and II (1917 cycles), (c) mechanism II (376 cycles), and (d) large-scale buckling (1830 cycles) where BC surface imperfections were eliminated before TC deposition [22].

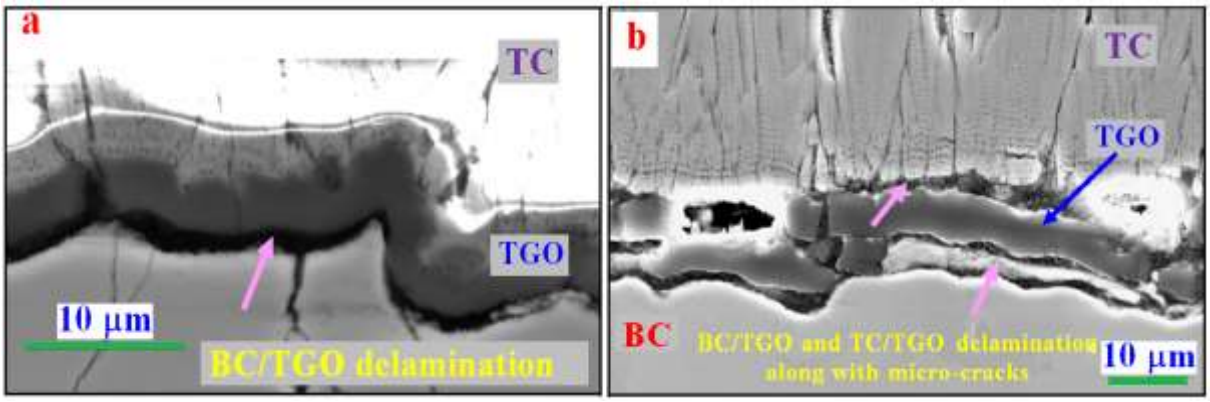

Fig. 14. BC/TGO delamination (a) after 1000 hours at 1000 ˚C/σmax = 160 MPa, (b) after 1168 hours at 1050 °C/ σmax = 130 MPa. White arrows highlight the TGO/BC delamination along with some micro-cracks propagating within the BC. Micro-cracking is observed at both the TC/TGO and TGO/BC interfaces in (b) [62].

3.3 Thermal Fatigue

Thermal fatigue during operation as temperature transition occurs slowly and repeatedly. TBCs aresubjected to thermal gradients in several ways[63].

Firstly, the gradient is set up along the thickness direction because of active cooling at the back of the TBC. Secondly, along the surface direction, the gradient occurs due to non-uniformity in the heating/cooling process in the hot components like combustion chambers. Thirdly, engine shut-off/starting can cause gradients. In addition to the

thermal response, mechanical loading also imparts stress gradients across the thickness and cyclic nature of loading. Therefore, the response of TBCs to thermo-mechanical loading and stress gradients is the most important issue. The thermal cyclic fatigue test is carried out by raising the temperature of TBC to a high temperature (approximately 1200 °C) and holding it for a fixed period (about one h), then cooling it to a low temperature (RT or 100 °C) and waiting for 10 min before beginning the next cycle. The damage and ultimate failure in TBC systems under thermal fatigue occur by the spallation of the ceramic TC, and the resistance is measured by the number of cycles sustained by TBC for around 20%-30% of surface spallation. Thermal cycling brings considerable changes in the microstructures in TBC because of sintering effects. Significant changes in microstructure include the formation and growth of TGO due to oxidation; changes in the shape, size, and number of pores due to healing; crack initiation; growth, and coalescences. Horizontal cracks generally form along the interfacial region between the TGO and the YSZ coat, but transverse cracks gradually develop with continued sintering effects [64]. With several cycles around 700 and higher, cracks eventually spread inside the TGO and the YSZ coat, forming a network of cracks. The network is mainly responsible for delamination when little TBC life is expected. Cracks also form around the surface roughness crest during thermal cycling. The damage developed in the TBC with thermal cycling due to crack networking is also accompanied by a transformation in the microstructure. It eventually extends to the BC, TC, and TGO regions. The spallation damage begins around the edge/corner of the TC at different cycles. Eventually, the damage spreads to other regions when delamination to spallation occurs.

3.4. YSZ phase Transformation and Stiffening (Sintering)

For higher energy efficiency, the temperature of the turbine inlet gas might be increased. When the service temperature reaches 1200 °C, the YSZ TBC undergoes mechanical degradation due to sintering. Sintering is caused by the connection between ceramic splats and is driven by the surface energy reduction of the whole system. This results in changes in mechanical and microstructural properties [65]. The defects, particularly two-dimensional cracks and pores would vanish for the free surface or interface to be reduced. In APS-TBC, pores are present between successive layers of deposit (intersplat), and numerous micro-cracks are also present within each layer (intra-splat) [66]. Prolonged sintering healing of defects occurs. It degrades the quality of TBC because, as the elongation increases by 80 % of the bulk material, the strain tolerance of TC decreases, enhancing the tendency for spallation [67, 68]. Phase stability becomes an issue because of sintering at a temperature over 1200 °C. Long sintering has another effect when martensitic phase (m-ZrO_2) transformation occurs from the tetragonal to the monoclinic phase. Around 5% to 7% volume change is accompanied by this transformation when residual stress builds up, causing cracking and the spallation of the TC. In addition, this phase change is responsible for an increase in thermal conductivity, and a phase monoclinic has inherent higher conductivity [69-72].

3.5. Thermal Shock

Thermal shock resistance is the property of a material that makes it resistant to sudden and rapid temperature changes. When a material is heated or cooled rapidly, a temperature difference is created between the surface and center, resulting in stress induction. Materials with high thermal shock resistance properties can withstand broad temperature gradients. TBCs are subjected to thermal gradients arising out of several sources during service. Major sources may include active cooling from back side internal cooling, engine shut down causing faster cooling of the top surface, nonuniform heating and cooling [63]. Commonly thermal shock behavior is measured by heating TBCs to a high temperature in a furnace, holding them for 5–10 min, and then dropping them in water to quench them. The steps are repeated or cycled until any surface damage or failure is noticed. The number of repeated cycles until 10% to 20% spallation of the top surface is a measure of thermal shock [73]. Brittle ceramics' low thermal shock resistance is one of their weakest points. Some factors influence thermal shock resistance, such as thermal conductivity, CTE, Poisson's ratio, elastic modulus, and fracture toughness. Fig. 15. illustrates the stresses induced and the changes that occur under thermal shock conditions. In the figure, ΔT, Tp, and Tz represent temperature differences, the temperature at the surface of the specimen, and the temperature at its center, respectively [74]. The development of the residual stress in the TBCs during thermal shock has been simulated by Wang et al. [76]. Based on the results, the maximum residual stress is at the initial cooling stage in a thermal cycle. The stress concentration at the surface crack's tip is higher than that of the inner crack in the ceramic layer. Furthermore, the stress intensity factor is the highest. Additionally, in the small distance between the crack and its neighboring pores, the stress concentration is relieved by the pores leading to the delay in the crack initiation and reduction of its propagation rate. When there is a considerable distance, the influence of pores on the neighbored cracks is not evident.

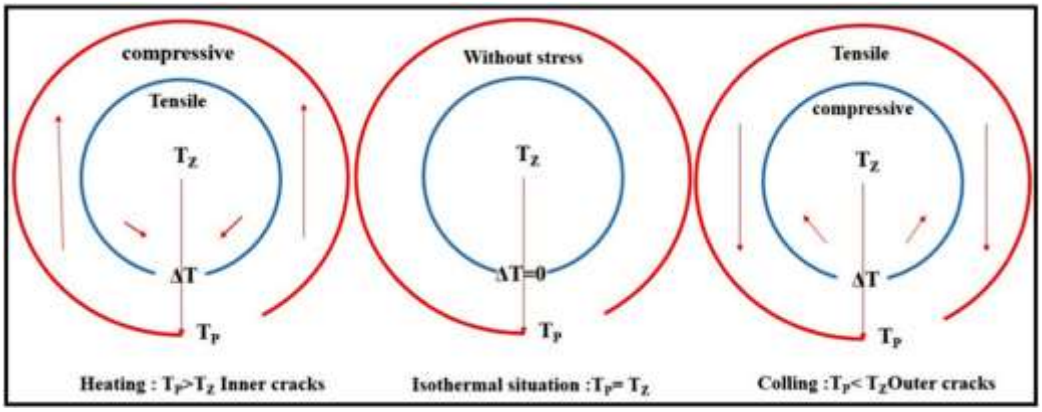

Fig. 15. Stresses developed under various thermal conditions [75].

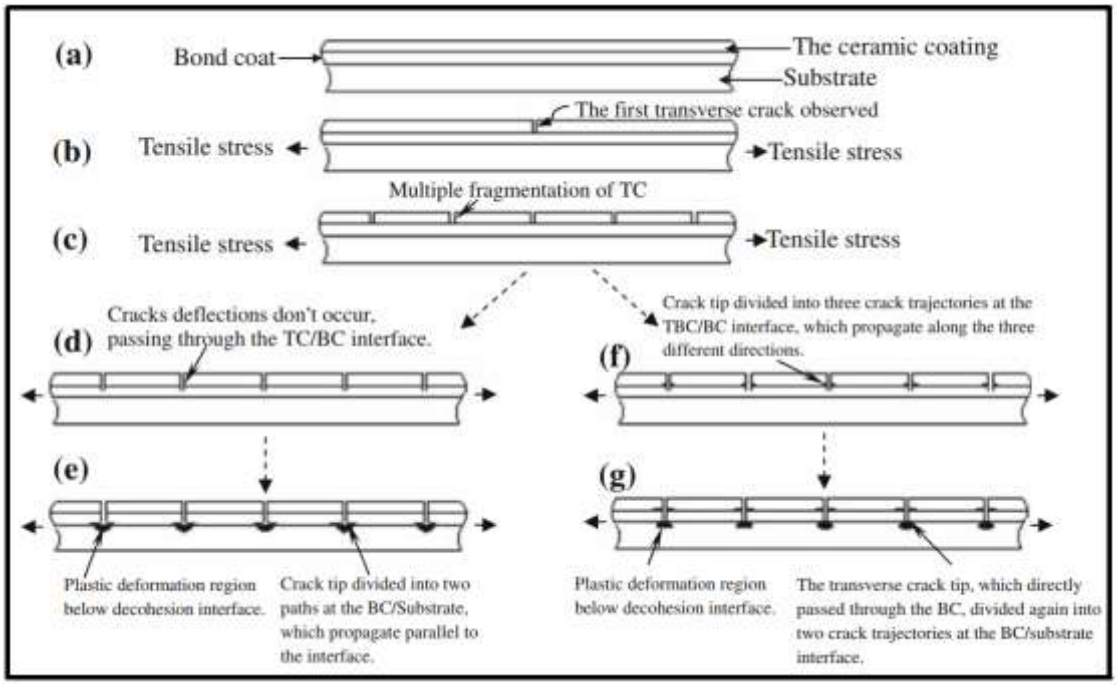

Fig. 16. Schematic diagram showing the damage evolution of the TBC system under the thermo-mechanical tensile loading [81].

4. Extrinsic Failure Mechanisms of YSZ TBC

4.1. Thermo-Mechanical Tensile

During thermal cycling, high stresses could be applied between the layers and their interfaces because of the large temperature gradient and CTE mismatch across the layers. These stresses cause the formation of cracks and spallation of the coatings [77]. The thermo-mechanical tensile failure with two different fracture characteristics is plotted in Fig. 16. Fig. 16.a-e denoted the first fracture behavior. The other failure process was described in Fig. 16.a-c, f, and g. Every failure characteristic was divided into five stages, i.e. (a) Pre-loading state; (b) with increasing tensile stress in the cooling stage, the first vertical crack initiation and transverse propagation in the ceramic TC layer; (c) more and more edge transverse cracks multiplication; (d) each crack tip did not deflect at the TC/BC interface and directly passed through the BC layer; (e) this transverse crack approached the BC/substrate interface and was divided into two parallel interface crack, which propagated along the BC/substrate interface. All cracking began to saturation in the BC/substrate interface [78, 79]. However, the other failure mode, i.e. (f), was also found when cracks passed through the interface between the TC and BC layers and deflected into three different trajectories. Both of them propagated parallel to the TC/BC interface. Another continued penetrating the BC layer perpendicular to the TC/BC interface (g), the transverse crack deflection and growth at the BC/substrate interface. So the (a)→(b)→(c)→(d)→(e) and (a)→(b)→(c)→(f)→(g) five-stages model, respectively, describe the two different fracture characteristic. The former characteristic was that multiple tensile cracks initiated on the surface of

the TC propagated towards the TC/BC interface and deflected at the BC/substrate interface. The fracture position is located within the BC layer near to the BC/substrate interface. The later fracture behavior was that the multiple tensile cracks also initiated on the surface of the TC, propagated towards the TC/BC interface. But transverse cracks deflected at the TC/BC and BC/substrate interfaces. The interface cracks within the TC layer, propagating parallel to the TC/BC interface, finally resulted in the spallation of the ceramic coating. Transverse cracks in the TC layer were expected to deflect at the interface between the TC and BC because the BC is a metal. This fracture phenomenon in the present work consists of the previous results for brittle coating [80].

4.2. Erosion

TBCs are more affected by erosion damage, which leads to material removal, followed by structural failure of the gas turbine engine components. The processing techniques of TBCs strongly influence erosion mechanisms. APS-TBC coating shows horizontally arranged splat microstructure which is relatively easy to remove since it contains many oriented cracks and particle boundaries parallel to the surface. In the case of EB-PVD TBCs, a new crack surface must be formed across the individual column at a much higher energy level. It has been noticed that EB-PVD TBCs provide better erosion resistance than APS TBCs [82].

Several mechanisms contribute to the erosion of TBCs. Three factors affect these mechanisms: 1) size of impacting particles; 2) microstructure variation resulting from the coating methods (APS or EB-PVD); 3) temperature of the impacting particle in the form of solid particles or semi-molten state; 4) velocity and density of the small particles or foreign objects; and 5) impingement angle of the particle. Erosion of TBCs deposited by EB-PVD is categorized into two mechanisms: foreign object damage (FOD) and near-surface cracking [83]. Mapping the conditions that contribute to these mechanisms has been done and is associated with particle size and velocity [84]. The contributing mechanisms are illustrated schematically in Fig. 17. The damage mechanisms can be described as follows.

Mode I – Erosion (near-surface cracking or lateral cracking):

Engines usually generate small, low-energy particles when operating. When these particles impact the TBC coating, cracks are formed near the surface of individual columns (top 20 μm). If several neighboring columns are impacted and cracked, material loss is observed. Under the impacting particles, the crack initiation occurs at the elastic/plastic transition [83].

Mode II - Compaction damage:

Compaction damage is intermediate between FOD and small particle erosion. This mechanism could be a transition stage between the two mechanisms. This state happens when the TBC columns present in EB-PVD coatings are compacted. However, this mechanism does not observe the near-surface cracking in Mode I or the gross plastic deformation and cracking in Mode III. Columns are compacted but not fractured due to the lower stain rates of the impact and the high porosity in the columns. The density of these coatings is less than 90 %. In mode I, a similar compacting occurs where one or two columns are only subjected to near-surface damage, and lateral cracking is initiated from the elastic/plastic interface. Nevertheless, the initiation of cracks does not occur at this interface when many columns are exposed to impact (Mode II). It is suggested to be the result of a lower strain rate originating from a lower energy input rate by the decelerating particle [85].

Mode III - Foreign object damage (FOD):

FOD results from smaller particles with high velocities or larger particles with low and intermediate velocities. In this condition, the gross plastic deformation of the columns in the coating is observed, which can penetrate the substrate. When significant, slow-moving particles impact the high-velocity rotating turbine blades, FOD damage may occur.

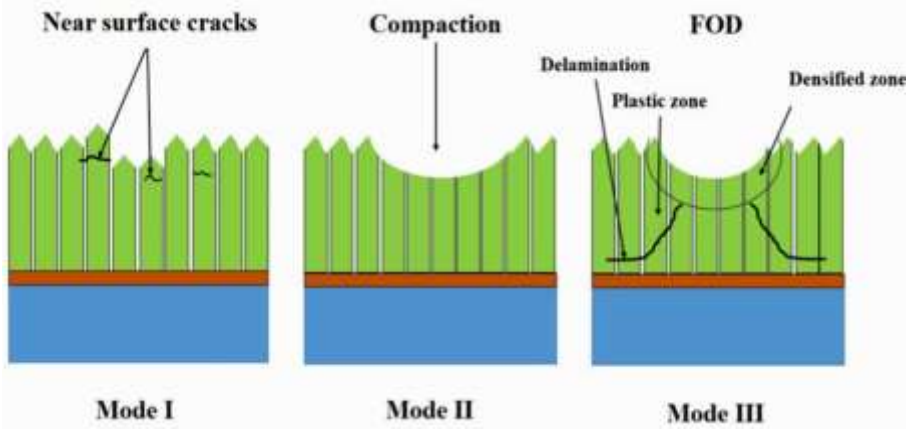

Fig. 17. Mechanisms of EB-PVD TBCs erosion [83].

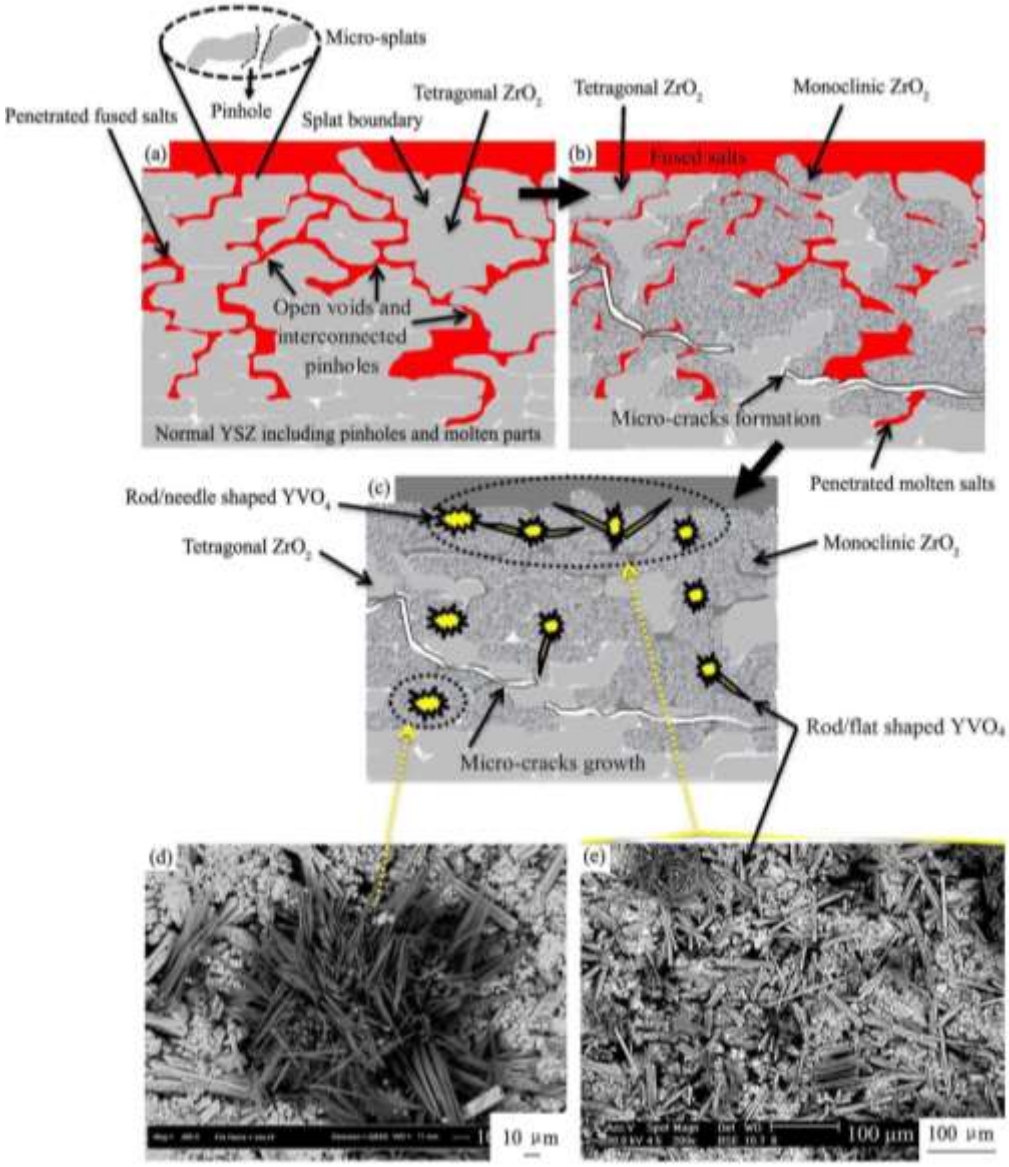

Fig. 18. Schematic illustration of hot corrosion process in YSZ layer (including fully molten parts), (a) Penetrated corrosive fused salts (with further penetration) into the entire thickness of the YSZ layer; (b) Depletion of stabilizer (Y2O3) in ZrO2 and followed by the phase transformation of t- ZrO2 to m- ZrO2; (c) Faster transformation of ZrO2 to fully monoclinic and formation of YVO4 crystals with outward growth; (d, e) FE-SEM and SEM images of YVO4 crystals at different magnifications [91].

4.3. Chemical attack by molten salts (Hot corrosion)

Hot corrosion is known as corrosion resulting from molten salts in the environment of an oxidizing gas at high temperatures. Hot corrosion occurs when salt films cover the surface of metals and alloys at the temperature range of 700-925 ˚C. Alkali and alkaline earth sulfates are salts [86-88]. Hancock proposed that the sulfur compounds and sodium chloride reaction in the surrounding gas phase results in sulfate deposits. The temperature between 700-900 ˚C and the presence of these deposits accelerates the oxidation process called ‘‘hot corrosion” [89]. Various factors, such as coolant, air compositions, fuel impurities, and particular industrial processes influence the exact composition of these salts. Fuel oils and coal contain sulfur which can yield SO2 on combustion and then transform to SO3 by partial oxidation. Na2SO4 is formed by reacting SO3 and water vapor with NaCl (an impurity in the air/fuel). This product deposits on the surface of metal or alloy and can be liquid at a relatively high temperature. Highly corrosive sodium vanadates with a low melting point are formed by reacting V2O5 (produced on combustion from small amounts of V in the fuel) and Na2SO4. The melting point of Na2SO4 is 884 ˚C. Therefore, it causes accelerated attacks on the Co and Ni-based superalloys at high temperatures.[90]

Corrosions above the salt’s melting point and at the lower temperature range values are called ‘‘type I

hot corrosion" and ''type II hot corrosion," respectively. In both hot corrosion types, the protective oxide layer on the surface of coatings and superalloys is adversely affected by fluxing with corroding salts. Consequently, internal sulfidation and oxidation are initiated when the protective layer becomes ineffective. Hot corrosion has been found to have two stages: 1) broken down of the protective oxide layer (initiation stage); 2) accelerated corrosion and deterioration process due to the access of the salts to the unprotected metal (propagation stage) [92-94].

The Schematic illustration of the hot corrosion process in the conventional YSZ layer is shown in Fig. 18. The molten salts can diffuse into the coating through cracks and pores, leading to the reaction with BC. Moreover, the chemical reaction between the stabilizing phases of YSZ and deposits leads to the accelerated sintering of zirconia and/or the formation of monoclinic zirconia from the tetragonal phase resulting in the degradation of TBCs [95-97]. Both events cause an increase in stress build-up in the zirconia layer. Young's modulus of the zirconia coating increases due to sintering, hence a decrease in the mechanical properties. Furthermore, additional stresses could be applied to the coating due to the thermal expansion mismatch between zirconia and infiltrated molten deposits [98].

4.4. Calcium-Magnesium–Aluminum-Silicate Environmental Attack (CMAS Attack)

Calcium -magnesium–aluminum-silicates (CMAS) environmental attack results from of mineral debris containing silica, such as dust, sand, and ash, entering the engine during the operation [99]. Due to the penetration of the molten CMAS into the porosity of APS-deposited YSZ or the inter-columnar spaces of EB-PVD-deposited YSZ, yttrium from the coating is depleted. Additionally, the solidification of the molten CMAS during cooling stages occurs, and TC faces the loss of strain tolerance resulting from the formation of the monoclinic zirconia phase (depletion of yttrium), the unwanted glass, which accelerates TBCs failure. CMAS also induces partial removal of TC. Upon rapid heating, residual stresses are induced on the top of YSZ, causing a vertical crack (mode I in Fig. 19). During rapid cooling, in-plane cracks are also formed, which depends on the penetration depth of the CMAS.

Generally, the degradation steps of thermal barrier coating by CMAS are as follows:

1. At high temperatures, CMAS is deposited on top of the TBC and penetrates below the surface into the columnar structure.
2. The penetration causes vertical cracks in the thermal barrier coating (mode I).
3. Due to the significant thermal stresses near the CMAS deposited surface and the penetration of CMAS, in-plane cracks parallel to the surface are induced below the TBC surface.
4. CMAS deposited might partially melt when the temperature increases beyond 1400˚C because the melting temperature of CMAS is around 1200 ˚C [100]. Due to capillary pressure, CMAS melt could enter into the in-plane cracks. As a result of the thermal expansion of CMAS particulates in the vicinity of the tip of the crack, further propagation of the CMAS-filled cracks could occur. The YSZ top coat is partially removed due to the joining of two adjacent cracks [29].

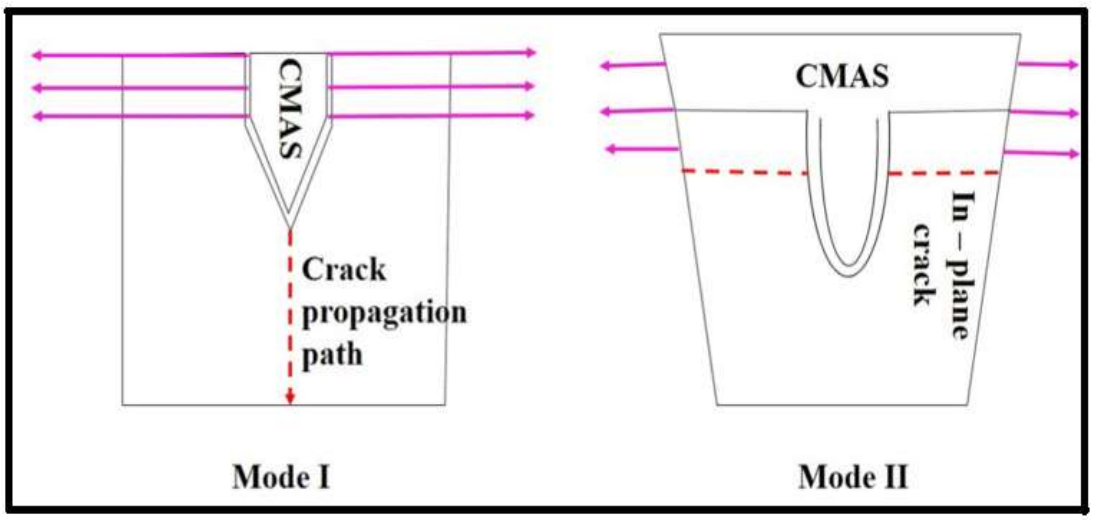

Fig. 19. Mechanisms of crack initiation and propagation by CMAS.

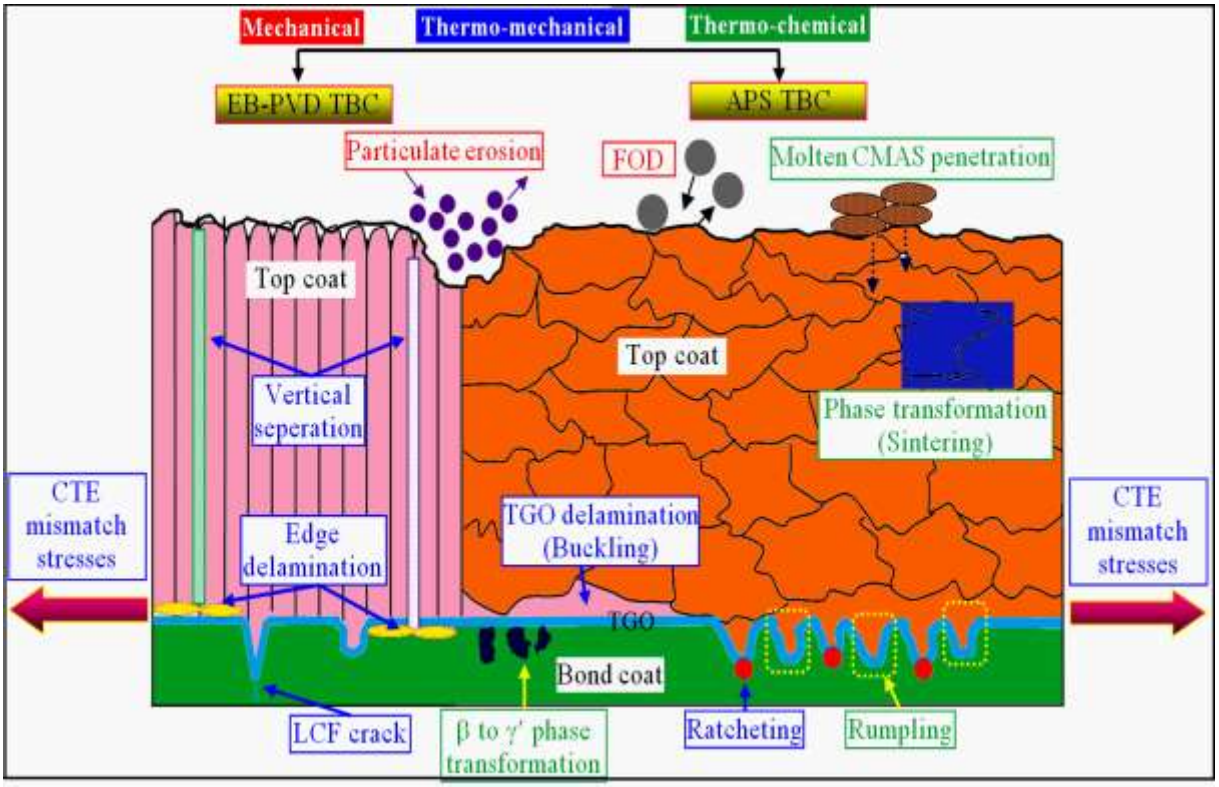

Fig. 20. Shematic illustration of degradation mechanisms of APS and EB-PVD-TBCs.

5. Conclusion

The stress generation in TBC due to various sources is the driving force for spallation failure. In the present article, some critical degradation modes of APS-TBCs and EB-PVD TBCs were discussed as follows, and the schematic illustration of them is shown in Fig. 20. :

(a) CTE mismatch and thermo-mechanical stress: Engine start-ups, load changes, and shutdown cause thermal cycling. Adjacent layers in TBC systems are subjected to repeated stress fluctuations because of CTE mismatch. This stress cycling leads to micro-crack initiation at and near the interface region. Micro-cracks are unevenly distributed and tend to extend horizontally and vertically to cause the delamination of the coating.

(b) TGO growth, roughness, and ratcheting: Uneven growth of TGO on the rough BC/TC interface during isothermal and cyclic exposure at high temperatures occur. Exponential TGO growth at peaks and valleys and around the thick TGO region develops stresses of opposite natures to a large magnitude.The stress situation due to TGO growth worsens in the presence of a temperature gradient due to CTE mismatch. The extent of TGO growth even affects the crack propagation path and mode along BC/TGO and TC/TGO interfaces. TGO thickness plays a significant role in shortening the TBC life. A critical thickness of TGO triggers the failure of TBCs by spallation. With oxidation, cracking occurs in the BC/TGO interface and TC to cause spallation in APS TBC. The inhomogeneous temperature field revealed the uneven growth of the

TGO layer with a rough surface. In other words, a rough interface leads to the uneven growth of TGO, and uneven growth leads to the increased roughness of TGO. The roughness of TBCs has a significant impact on stress distribution, the failure mechanism, and service lifetime. Many types of research demonstrated the dependency of TGO thickness and the resulting residual stress on the roughness in the TBC peak and valley regions. Considerable stress develops due to CTE mismatch, and TGO growth stress leads to delamination, different crack formation, and failures in smooth EB-PVD TBC and rough APS TBC.

The formation and growth of the □-Al2O3 TGO results in the depletion of Al in the BC. The Al depletion, if severe, forms of other oxides, such as Ni- and Co-containing spinels. The formation of these phases compromises the structural integrity of the TGO and accelerates localized oxidation by providing fast oxygen-diffusion paths. During thermal cycling, progressive roughening of the BC/TGO/TC interfaces occurs due to the cyclic creep of the BC. Such roughening, often termed “ratcheting,” requires thermal cycling and does not occur during isothermal exposures. It also requires an initial surface-geometry imperfection of some minimum dimension and the progressive lengthening of the TGO either due to TGO cracking or in-plane growth during oxidation. For a

nominally flat BC/TGO interface (EB-PVD TBC), this roughening manifests in the form of TGO penetration into the BC. The undulation amplitude is amplified in an already undulated interface (APS TBC). These geometrical factors result in out-of-plane stresses normal to the metal/ceramic interface, the severity of which increases with thermal cycling. These stresses, in combination with the interfacial imperfections, are primarily responsible for TBC degradation. Damage initiation and progression in micro-cracks can occur in many different ways in TBCs, depending on the particular TBC, the portion of spallation life already consumed, and the thermal cycling environment. The coalescence of these cracks results in the ultimate spallation failure of the TBC .
(c) Buckling: The residual stress distribution present in TBC reaches a level to cause the buckling of the TC layer. It favors easy crack initiation and propagation, followed by the spallation of the ceramic TC layer.
(d) BC and TC Phase transformations: The phase transformation of BC near the TC/BC interface plays a dominant role in the degradation of interfacial adhesion. In particular, the coexistence of γ□ and martensitic phases, each having a very different thermo-mechanical response under thermal exposure, can generate misfit stress in the TGO layer and ultimately cause early TBC spallation. In addition, the phase transformation behavior has been closely associated with the inherent chemistry of the BC and substrate. Also, above 1200 ˚C, a diffusionless phase transformation from metastable tetragonal (t′-ZrO2)-phase to tetragonal (t- ZrO2) and cubic (c) phase occurs above that temperature. This tetragonal phase transforms into a monoclinic phase with a high volume change during cooling, and this phenomenon causes severe
damages in the coating.
(e) Sintering: Properties and microstructure of the TC change during the sintering process. Thermal conductivity and elastic modulus increase significantly. Increased elastic modulus of the TC due to sintering will reduce the strain tolerance of the coating and the coating life. The porosity of the coating decreases due to sintering occurring above 1200 ˚C, and thermally induced stresses come into existence. Failure possibility increases on the YSZ-based TBC due to these stresses. Porous YSZ becomes stiffer and less compliant because of sintering at a high temperature. Thermal shock during cooling can cause transverse cracking across the layer.
(f) Mechanical damage by erosion: The particulate erosion of TBCs is caused by sliding or the impact of solids, liquids, or a combination of these elements. The mechanisms involve impingement, particle, and materials variables. The impingement variables mainly consist of particle velocity, particle concentration, and angle of incidence. The particle variables include particle shape, size, etc. Materials variables involve material properties, such as hardness and porosity in TBCs.
(g) Hot corrosion and CMAS attack: The TBC system is exposed to various gases and solids during operation, such as CO2, SO2, molten salts like alkali and alkaline earth sulfates or vanadates (Na2SO4 and V2O5), chlorides, and solid particles in the form of sand and fly ashes. Hot corrosion is a chemical reaction between the metal and molten salts in a hot oxidizing condition. Corrosive deposits can also seriously erode moving engine parts, including the compressor and turbine blades, thus reducing engine efficiency. Molten salts can solidify inside cooling passages, clogging the passages and reducing cooling airflow, increasing blade and vane operating temperatures, and shortening the engine life. TBC degradation can also occur due to the penetration of sulfide sediments and air sands. Also, YSZ can be quickly and seriously damaged by Ca-Mg-Al-silicate (CMAS) attacks caused by flying ash .
CMAS attack causes deterioration and spallation of the coating.

References

[1] A.H. Pakseresht, A.H. Javadi, M. Nejati, K. Shirvani, E. Ghasali and R. Teimouri, J. Adv. Manuf. Technol. ,75(2014), 739.
[2] P.A. Hossein, M.R. Rahimipour, M. Alizadeh, S.M.M. Hadavi and A. Shahbazkhan: Concept of Advanced Thermal Barrier Functional Coatings in High Temperature Engineering Components, Research Perspectives on Functional Micro- and Nanoscale Coatings, Hershey, USA, (2016), 396.
[3] A.G. Evans, D.R. Mumm, J.W. Hutchinson, G.H. Meier and F.S. Petit, Prog. Mater. Sci. , 46(2001), 505.
[4] A. Jam, S.M.R. Derakhshandeh, H. Rajaei and A.H. Pakseresht, Ceram. Int. , 43(2017), 14146.
[5] X.S. Li, W.W. Cai, J.H. An, S. Kim, J. Nah, D.X. Yang, R. Piner, A. Velamakanni, I. Jung, E. Tutuc, S.K. Banerjee, L. Colombo and R.S. Ruoff, Science, 324(2009), 1312.
[6] X.S. Li, W.W. Cai, L. Colombo and R.S. Ruoff, Nano Lett. , 9(2009), 4268.
[7] K.S. Kim, Y. Zhao, H. Jang, S.Y. Lee, J.M. Kim, J.H. Ahn, P. Kim, J.Y. Choi and B.H. Hong, Nature, 457(2009), 706.
[8] W.W. Cai, Y.W. Zhu, X.S. Li, R.D. Piner and R.S. Ruoff, Appl. Phys. Lett. , 95(2009), 123115.
[9] A. Pakseresht, M. Saremi, H. Omidvar and M. Alizadeh, Surf. Coat. Technol. , 366(2019), 338.
[10] L. Chen, Surf. Rev. Lett. , 13(2006), 535.
[11] C.U. Hardwicke and Yuk-Chiu Lau, J. Therm. Spray Technol. , 22(2013), 564.
[12] V. Akdogan, M.M. Dokur, G. Goller and O. Keles, J. Mater. Eng. Perform. , 22(2013), 2500.

[13] M.G. Gok and G. Goller, J. Eur. Ceram. Soc., 36(2015), 1755.
[14] S. Mahade, N. Curry, S. Bjorklund, N. Markocsan and P. Nylen, J. Alloys Compd., 689(2016), 2.
[15] G. Mauer, M.O. Jarligo, D.E. Mack and R. Vaßen, J. Therm. Spray Technol. , 22(2013), 646.
[16] J. H. Park, J. S. Kim, K.H. Lee, Y.S. Song and M.C. Kang, J. Mater. Process. Technol., 201(2008), 331.
[17] B.S. Senturk, H.F. Garces, A.L. Ortiz, G. Dwivedi, S. Sampath and N.P. Padture, J. Therm. Spray Technol. , 23(2014), 708.
[18] M.G. Gok and G. Goller, Surf. Coat. Technol., 276 (2015), 202.
[19] M.G. Gok and G. Goller, J. Eur. Ceram. Soc., 37(2017), 2501.
[20] D. Stover, G. Pracht, H. Lehmann, M. Dietrich, J.E. Doring and R. Vaben, J. Therm. Spray Technol., 13(2004), 76.
[21] D. Chellaganesh, M.A. Khan and J.T.W. Jappes, Mater. Today Proc. , 45(2021), 1529.
[22] N.P. Padture, M. Gell and E.H. Jordan, Science, 296(2002), 280.
[23] T.E. Strangman, Thin Solid Films, 127(1985), 93.
[24] M. Peters, K. Fritscher, G. Staniek, W.A. Kaysser and U. Schultz, Materwiss Werksttech., 28(1997), 357.
[25] A. Kumar, J. Moledina, Y. Liu, K. Chen and P.C. Patnaik, Coatings, 11(2021), 1474.
[26] A. Bolcavage, A. Feuerstein, J. Foster and Peter Moore, J. Mater. Eng. Perform. , 13(2004), 389.
[27] D. Liu, M. Seraffon, P.E.J. Flewitt, N.J. Simms, J.R. Nicholls and D.S. Rickerby, J. Eur. Ceram. Soc. , 33(2013), 3345.
[28] A. Rabiei and A.G. Evans, Acta mater. , 48(2000), 3963.
[29] R.T. Wu, M. Osawa, T. Yokokawa, K. Kawagishi and H. Harada, J. solid mech. mater. eng. , 4(2010), 119.
[30] G.H. Meng, H.Liu, M.J. Liu, T. Xu, G.J. Yang, C.X. Li and C.J. Li, Corros. Sci., 163(2020),108275.
[31] A.J. Haynes, D.E. Rigney, M.K. Ferber and W.D. Porter, Surf. Coat. Technol. , 87(1996), 102.
[32] H. Dong, G.J. Yang, C.X. Li, X.T. Luo and C.J. Li, J. Am. Ceram. Soc. , 97(2014), 1226.
[33] O. Trunova, T. Beck, R. Herzog, R. Steinbrech and L. Singheiser, Surf. Coat. Technol., 202(2008), 5027.
[34] Y. Bai, C. Ding, H. Li, J. Therm. Spray Technol. , 22(2013), 1201.
[35] H. Hindam and D.P. Whittle, Oxid. Met. , 18(1982), 245.
[36] Z. Mutasim, C. Rimlinger and W. Brentnall, Am. Soc. Mech. Eng. , 53(1997), 1.
[37] V.K. Tolpygo and D.R. Clarke, Acta Mater. , 48(2000), 3283.
[38] R. Eriksson, H. Brodin, S. Johansson, L. Östergren and X.H. Li, Surf. Coat. Technol., 205(2011), 5422.
[39] V. Sergo and D.R. Clarke, J. Am. Ceram. Soc., 81(1998), 3237.
[40] J .W. Hutchinson and Z. Suo, Adv. Appl. Mech., 29(1992), 63.
[41] W. Peng and D.R. Clarke, J. Am. Ceram. Soc., 83(2000), 1165.
[42] B.Y. Zhang, G.J. Yang, C.X. Li and C.J. Li, Appl. Surf. Sci., 406(2017), 99.
[43] D.M. Lipkin and D.R. Clarke, Oxid. Met. , 45(1996), 267.
[44] D.R. Clarke, Curr. Opin. Solid State Mater. Sci., 6(2002), 237.
[45] D.R. Clarke and C.G. Levi, Mater. Res., 33(2003), 383.
[46] V. Kumar and K. Balasubramanian, Prog. Org. Coat. , 90(2016), 54.
[47] R.A. Miller and C.E. Lowell, Thin Solid Films, 95(1982), 265.
[48] K.W. Schlichting, N.P. Padture, E.H. Jordan and M. Gell, Mater. Sci. Eng. A, 342(2003), 120.
[49] X.Y. Gong and D.R. Clarke, Oxid. Met. , 50(1998), 355.
[50] D.R. Clarke and W. Pompe, Acta Mater. , 47(1999), 1749.
[51] C.H. Hsueh, P.F. Becher, E.R. Fuller, S.A. Langer and W.C. Carter, Mater. Sci. Forum, 442(1999), 308.
[52] C.H. Hsueh and E.R. Fuller, Scripta Mater. , 42(2000), 781.
[53] K. Vaidyanathan, M. Gell, E.H. Jordan, Surf. Coat. Technol. , 133(2000), 28.
[54] A.G. Evans, M.Y. He and J.W. Hutchinson, Prog. Mater. Sci. , 46(2001), 249.
[55] Y.H. Sohn, J.H. Kim, E.H. Jordan and M. Gell, Surf. Coat. Technol. , 146(2001), 70.
[56] D.R. Mumm and A.G. Evans, Acta Mater. , 48(2000), 1815.
[57] M. Gell, Surf. Coat. Technol. , 120(1999), 53.
[58] J. Cheng, E.H. Jordan, B. Barber and M. Gell, Acta Mater. , 46(1998), 5839.
[59] A.G. Evans and J.W. Hutchinson, Int. J. Solids Struct. , 20(1984), 455.
[60] T. Xu, M. He and A. Evans, Acta Mater. , 51(2003), 3807.
[61] S. Wen and S. Zhou, Adv. Mech. Eng., 10(2018).
[62] F. Riallant, J. Cormier, A. Longuet, X. Milheta and José Mendez, Metall. Mater. Trans. A, 45(2014), 351.
[63] C. Zhang and C. Chen: Failure mechanism of thermal barrier coatings by electron beam physical vapor deposition (EB-PVD) under thermo-mechanical coupled loads. In Thermal Barrier Coatings Woodhead Publishing Series in Metals and Surface Engineering: Cambridge, UK, (2011), 215.

[64] G. Bolelli, M.G. Righi, M.Z. Mughal, R. Moscatelli, O.Ligabue, N. Antolotti, M.Sebastiani, L. Lusvarghi and E. Bemporad, Mater. Des. , 166(2019), 107615.
[65] B. Cheng, Y.M. Zhang, N. Yang, M. Zhang, L. Chen, G.J. Yang, C.X. Li, C.J. Li, J. Am. Ceram. Soc. , 100(2017), 1820.
[66] S. Kyaw, A. Jones and T. Hyde, Eng. Fail. Anal. , 27(2013), 150.
[67] Z. Wu, L. Ni, Q. Yu and C. Zhou, J. Therm. Spray Technol. , 21(2012), 169.
[68] L.S. Wang, Z.Y. Wei, B. Cheng, M.J. Liu, G.R. Li, H. Dong and G.J. Yang, Ceram. Int. , 46(2020), 2355.
[69] C. Xing, M. Yi, X. Shan, X. Wang, X. Zhao and F. Guo, J. Am. Ceram. Soc. , 103(2020), 7267.
[70] Y. Zhao and Y. Gao, Appl. Surf. Sci. , 425(2017), 1033.
[71] J. Wu, H. Guo, L. Zhou, L. Wang and S. Gong, J. Therm. Spray Technol. , 19(2010), 1186.
[72] L. Bowen, H. Xie, R. Xu, X.L. Fan, W.X. Zhang and T.J. Wang, Appl. Surf. Sci. , 360(2016), 461.
[73] R.S. Lima and B.R. Marple, Mater. Sci. Eng. A, 485(2008), 182.
[74] E. Benini: Progress in Gas Turbine Performance, IntechOpen, Padula, Italy, (2013), 251.
[75] A. Pakseresht, F. Sharifianjazi, A. Esmaeilkhanian, L. Bazli, M.R. Nafchi, M. Bazli and F. Baharan, Mater. Des. , 222(2022), 111044.
[76] L. Wang, Y. Wang, W.Q. Zhang, X.G. Sun, J.Q. He, Z.Y. Pan and C.H. Wang, Appl. Surf. Sci. , 258 (2012), 3540.
[77] X. Fan, R. Xu, W. Zhang and T. Wang, Appl. Surf. Sci. , 258(2012), 9816.
[78] L. Qian, S. Zhu, Y. Kagawa and T. Kubo, Surf. Coat. Technol. , 173(2003), 178.
[79] D.M. Gray, Y.C. Lau, C.A. Johnson, M.P. Borom, and W.A. Nelson: Thermal Barrier Coatings Having an Improved Columnar Microstructure, US 6, 306, 517, (2001).
[80] M. Wen, E.H. Jordan and M. Gell, Surf. Coat. Technol. , 200(2006), 5193.
[81] W.G. Mao, C.Y. Dai, L. Yang and Y.C. Zhou, Int. J. Fract. , 151(2008), 107.
[82] M. Peters, C. Leyens, U. Schulz, W.A. Kaysser, Adv. Eng. Mater. , 3(2001), 193.
[83] R.G. Wellman, J.R. Nicholls, Wear, 242(2000), 89.
[84] J.R. Nicholls, Y. Jaslier and D.S. Rickerby, Mater. Sci. Forum, 251(1997), 935.
[85] R.G. Wellman, J.R. Nicholls, Tribol. Int. , 41(2008), 657.
[86] T. Sidhu, S. Prakash, R. Agrawal, Curr. Sci. , 90(2006), 41.
[87] Z.G. Liu, J.H. Ouyang, Y. Zhou and X. Xia, J. Eur. Ceram. Soc. , 29(2009), 2423.
[88] Z.G. Liu, J.H Ouyang, Y. Zhou and S. Li, J. Eur. Ceram. Soc. , 30(2010), 2707.
[89] P. Hancock, Mater. Sci. Technol. , 3(1987), 536.
[90] A.D. Gledhill, K.M. Reddy, J.M. Drexler, K. Shinida, S. Sammpath and N.P. Padture, Mater. Sci. Eng. A, 528(2011), 7214.
[91] M. Daroonparvar, M. Azizi Yajid, N. Yusof, H. Bakhsheshirad, E. Hamzah, M. Nazoktabar, J. Rare Earths. , 32(2014), 989.
[92] S. Bose: High temperature coatings, Butterworth-Heinemann, (2017), 199.
[93] A. Rabieifar, S. Nategh, M.R. Afshar and H. Najafi, Oxid. Met. , 94(2020), 549.
[94] A. Rabieifar, S. Nategh, M.R. Afshar and H. Najafi, Surf. Coat. Technol. , 439(2022), 128461.
[95] S. Park, J. Kim, M. Kim, H. Song and C. Park, Surf. Coat. Technol. , 190(2005), 357.
[96] M.H. Habibi, L. Wang and S. Guo, ASME, 3(2012), 905.
[97] M.H. Habibi, L. Wang and S.M. Guo, J. Eur. Ceram. Soc. , 32(2012), 1635.
[98] J. Wu, H.B. Guo, Y.Z. Gao and S.K. Gong, J. Eur. Ceram. Soc. , 3(2011), 1881.
[99] B. Zhang, W. Song and H.B. Guo, J. Eur. Ceram. Soc. , 38(2018), 3564.
[100] M. Borom, C. Johnson, L. Peluso, Surf. Coat. Technol. , 86(1996), 116.